Geophysical Research Letters

Supporting Information for

Rethinking the role of transport and photochemistry in regional ozone pollution: Insights from ozone mass and concentration budgets

K. Qu[1,2,3], X. Wang[1,2,*], X. Cai[1,2], Y. Yan[1,2], X. Jin[1,2], M. Vrekoussis[3,4,5], J. Shen[6], T. Xiao[1,2], L. Zeng[1,2] and Y. Zhang[1,2,7,8,*]

[1] State Key Joint Laboratory of Environmental Simulation and Pollution Control, College of Environmental Sciences and Engineering, Peking University, Beijing 100871, China.

[2] International Joint Laboratory for Regional Pollution Control, Ministry of Education, Beijing, 100816, China.

[3] Laboratory for Modeling and Observation of the Earth System (LAMOS), Institute of Environmental Physics (IUP), University of Bremen, Bremen, Germany.

[4] Center of Marine Environmental Sciences (MARUM), University of Bremen, Germany.

[5] Climate and Atmosphere Research Center (CARE-C), The Cyprus Institute, Cyprus.

[6] State Key Laboratory of Regional Air Quality Monitoring, Guangdong Key Laboratory of Secondary Air Pollution Research, Guangdong Environmental Monitoring Center, Guangzhou 510308, China.

[7] Beijing Innovation Center for Engineering Science and Advanced Technology, Peking University, Beijing 100871, China.

[8] CAS Center for Excellence in Regional Atmospheric Environment, Chinese Academy of Sciences, Xiamen 361021, China.

Corresponding author: X. Wang (xswang@pku.edu.cn) and Y. Zhang (yhzhang@pku.edu.cn)

Contents of this file

Introductions

Four texts, 12 figures and two tables are included in this Supporting Information for the paper entitled “Rethinking the role of transport and photochemistry in regional ozone pollution: Insights from ozone mass and concentration budgets”.

For text:

- Text S1 describes the detailed process of O_3 budget calculations in this study.
- Text S2 is the comparison between the equations of O_3 budget calculations used in this study with these in 1-D models.
- Text S3 presents the results of model validation of atmospheric boundary layer (ABL) height, wind and O_3 mixing profiles based on the IAGOS dataset.
- Text S4 gives further analyses on the contributions of horizontal transport and ABL-free troposphere (FT) exchange due to the large-scale air motions (ABL-FT-M; advection through the ABL top) in O_3 mass and concentration budgets.

For figures:

- Figure S1 indicates two calculation paths in the calculation of regional O_3 concentration budget within an hour.
- Figure S2 shows the results of O_3 budget closure examinations for O_3 mass and concentration budgets in the two representative months.
- Figure S3 displays the spatial distributions of the second modeling domain (d02) and source regions.
- Figure S4 presents the spatial distributions of 18 sites of the Guangdong-Hong Kong-Macao Pearl River Delta Regional Air Quality Monitoring Network.
- Figure S5 compared the mean diurnal changes of O_3 concentrations in the Pearl River Delta from three sources: observational near-ground O_3 concentrations, modeling near-ground O_3 concentrations and modeling ABL-mean O_3 concentrations.
- Figure S6 is the flow diagram of the O_3 budget calculation processes.
- Figure S7 is the flow diagram of the O_3 budget calculation in the Step I (or the tool *flux_4d_cal*).
- Figure S8 shows the comparison results between IAGOS and modeling atmospheric boundary layer height in Hong Kong in Oct. 2015.
- Figure S9 shows the comparisons between IAGOS and modeling wind roses in Hong Kong in the two representative months.
- Figure S10 shows the comparisons between IAGOS and CMAQ modeling vertical profiles of O_3 mixing ratios in Hong Kong in the two representative months.
- Figure S11 displays the wind roses at 14:00, 16:00, and 18:00 local time of O_3 polluted days in July 2016 in the Pearl River Delta.
- Figure S12 displays the cross-section of O_3 concentrations and wind fields at 16:00 local time on a representative polluted day of July 2016.

For tables:

- Table 1 gives more detailed information on the O_3 polluted days of the Pearl River Delta in the two representative months.
- Table 2 lists the formulas in the O_3 flux calculations, parameters used and their source files in the *flux_4d_cal* tool.

Text S1. Detailed process of O_3 budget calculations

As the flow diagram shown in Fig. S6, there are two steps in the calculations of O_3 budget based on the WRF-CMAQ modeling results:

1) Step I: Quantifications of transport fluxes and volume

The post-processing tool *flux_4d_cal* was developed using FORTRAN90 for this step. For all grids except for those next to the boundaries of the modeling domain, the calculation contents in the tool include:

- Hourly horizontal transport fluxes of O_3 within the ABL, including these in the x- and y-directions;
- Hourly fluxes of O_3 attributed to ABL-FT exchange due to the changes of ABL heights (ABL-FT-H);
- Hourly fluxes of O_3 attributed to ABL-FT exchange due to the large-scale air motion (advection through the ABL top; ABL-FT-M), including these in the x-, y- and z-directions;
- Hourly contributions of other processes (gas-phase chemistry, cloud process and dry deposition) to O_3 mass variations within the ABL;
- Hourly transported air volumes by each transport process;
- Total O_3 masses within the ABL at both the start and end of each hour;
- ABL heights at the starting and end hours.

(Note: ABL, atmospheric boundary layer; FT, free troposphere.)

All of the above values can be found in the netcdf (nc) output files, and they are used in the Step II calculations.

To finish the calculations of Step I, several input files are needed:

- Meteorological files processed by the MCIP module in CMAQ from the WRF outputs, which include the METCRO2D (meteorological parameters in the 2-D space), METCRO3D (meteorological parameters in the 3-D space) and MERDOT3D (wind speeds in the 3-D space) files;
- Pollutant concentration output files (CONC files) modeled by CMAQ, where hourly O_3 concentrations are stored;
- Process Analysis (PA) output files modeled by CMAQ, where the hourly, nested contributions of gas-phase chemistry, cloud process and dry deposition to O_3 concentration are stored.

For most of the files used here, the setting of spatial domains and times should be consistent; otherwise, the calculations would not be performed or generate wrong results. Additionally, users should provide the resolution of the modeling domain and the orders of contributions by three non-transport O_3 processes in the PA files for further calculations.

The flow chart of the calculation in *flux_4d_cal* is shown in Fig. S7. The calculation formulas for the grid cell (i, j), parameters used and their source files are summarized in Table S2. There are four loops in the calculations, which are the loops of x-, y-grids, time steps and vertical layers. We assume that there are 60 time-steps within an hour, and parameters at each time step can be

interpolated linearly by their values at the starting and end hours. The hourly contribution of non-transport processes to O_3 in a grid cell is divided equally to these within each time step. For every layer within the ABL, fluxes and volumes related to horizontal transport and non-transport processes are calculated and summed up. For layers where the ABL top is located, besides these aforementioned parameters, fluxes and volumes related to ABL-FT exchange (ABL-FT-H and ABL-FT-M) are also calculated. Total O_3 masses within the ABL at the start and end of each hour are directly calculated, and ABL heights at the starting and end hours can be read from the METCRO2D files.

The height of night-time stable ABL can be severely underestimated by normally used ABL parameterization, especially when the Richardson number is used (Dai et al., 2014). To reduce the influence of imprecise ABL heights in the O_3 budget calculations, here, we set the lowest ABL height limit as 350 m for all hours, which is an approximate value close to the values reported by night-time observations in summer or autumn in the Pearl River Delta (Chan et al., 2006; Fan et al., 2011; He et al., 2021; Song et al., 2021). The results of budget closure examination (Fig. S2) also suggest that the choice of this value is acceptable. Further studies are surely needed to better determine this value. However, we focus on the causes of daytime ozone pollution; thus, night-time budgets do not notably influence the conclusions of this study.

2) Step II: Regional O_3 budget calculations and closure examinations

This step aims to: 1) calculate the hourly O_3 mass and concentration budgets within the ABL of the user-defined regions, and 2) check whether the closure between the changes of O_3 masses/concentrations modelled by CMAQ and the net contributions of processes calculated above can be achieved. Besides the nc file generated in Step I, the definition of targeted region grids and borders (the grids within the targeted region and adjacent to the outside regions) should also be provided by users. Any software with basic data analysis and nc-file processing (Python, MATLAB, R, etc.) can be applied for this step.

The calculation processes in this step include:

- Calculation of the hourly horizontal transport fluxes of O_3 through each user-defined border (O_3 fluxes in every interface between the border grids and the outside regions, in both x- and y-directions, are taken into the calculations).
- Calculation of the hourly ABL-FT exchange fluxes of O_3 and the contributions of other processes to O_3 mass within user-defined targeted region grids.
- Calculation of the hourly O_3 concentration budget (the contributions of processes to the hourly variations of O_3 concentrations) based on O_3 transport fluxes and the corresponding volumes of transported air parcels.

More details on the calculation of the O_3 concentration budget are introduced as follows. As displayed in Fig. S1, within an hour, the mean O_3 concentration within the ABL of the targeted region changes from c_0 to c_1. Normally, O_3 mass and ABL volume both change notably, making it difficult to quantify the contributions to O_3 concentration variations by various processes. It should be noted that this is one of the main reasons why regional O_3 mass and concentration budgets are different. To simplify the calculation, two calculation paths (shown as the red arrowlines in Fig. S1; c_{r1} and c_{r2} are the reference O_3 concentrations separately for two calculation paths) are used in the calculations, assuming that only O_3 mass or ABL volume change in each step of two paths. For the path "c_0 => c_{r1} => c_1", the first step is the ABL volume change step, with O_3 concentration change described as:

$$c_{r1} - c_0 = c_0 \times \left(\frac{\sum H_0}{\sum H_1} - 1\right) \quad \text{(S1)}$$

where H_0 and H_1 are the ABL heights at the starting and end hours. It is counted as part of the contributions by ABL-FT-H. The second step is the O_3 mass change step, with O_3 concentration change described as:

$$\begin{aligned} c_1 - c_{r1} = & \frac{\sum(F_{htrans} - c_{r1} \times \Delta V_{htrans})}{L^2 \times \sum H_1} \\ & + \frac{\sum(F_{ABL-FT-M} - c_{r1} \times \Delta V_{ABL-FT-M})}{L^2 \times \sum H_1} + \frac{F_{ABL-FT-H}}{L^2 \times \sum H_1} \\ & + \frac{F_{chem}}{L^2 \times \sum H_1} + \frac{F_{cloud}}{L^2 \times \sum H_1} + \frac{F_{ddep}}{L^2 \times \sum H_1} \end{aligned} \quad \text{(S2)}$$

where F_{htrans}, $F_{ABL-FT-M}$, $F_{ABL-FT-H}$, F_{chem}, F_{cloud} and F_{ddep} indicate the contributions of horizontal transport, ABL-FT-M, ABL-FT-H, gas-phase chemistry, cloud process and dry deposition, respectively, to O_3 mass change. ΔV_{htrans} and $\Delta V_{ABL-FT-M}$ are the volumes of transported air parcel attributed to horizontal transport and ABL-FT-M, respectively, within an hour. L denotes the length of the grid cell, or the horizontal resolution of the model. The six terms on the right-hand sides of the above formula are separately classified as the individual contribution of horizontal transport, ABL-FT-M, ABL-FT-H, gas-phase chemistry, cloud process and dry deposition in the O_3 concentration budgets. Note that the contributions of ABL-FT-H are separately calculated in two steps. Similarly, for the path "c_0 => c_{r2} => c_1", the changes of O_3 concentration in two steps can be described as:

$$\begin{aligned} c_{r2} - c_0 = & \frac{\sum(F_{htrans} - c_0 \times \Delta V_{htrans})}{L^2 \times \sum H_0} \\ & + \frac{\sum(F_{ABL-FT-M} - c_0 \times \Delta V_{ABL-FT-M})}{L^2 \times \sum H_0} + \frac{F_{ABL-FT-H}}{L^2 \times \sum H_0} \\ & + \frac{F_{chem}}{L^2 \times \sum H_0} + \frac{F_{cloud}}{L^2 \times \sum H_0} + \frac{F_{ddep}}{L^2 \times \sum H_0} \end{aligned} \quad \text{(S3)}$$

$$c_1 - c_{r2} = c_{r2} \times \left(\frac{\sum H_0}{\sum H_1} - 1\right) \quad \text{(S4)}$$

The contributions of various processes can be classified correspondingly. The final results of contributions by processes are the average values of these calculated based on two calculation paths.

Text S2. Comparisons of O_3 concentration budget calculations between this study and 1-D models

When the region column in the Chemical Transport Models (CTMs) is thin enough to resemble a line, the O_3 concentration budget calculations using the CTMs results are expected to be the same as those in 1-D models. Thus, we can use it to check the validity of O_3 concentration budget calculations in this study.

Here the contributions of horizontal transport to the variations of O_3 concentration over the studied space ($\langle c \rangle$) can be described as (Eq. (3) in the manuscript):

$$\left[\frac{\partial \langle c \rangle}{\partial t}\right]_{htrans} = \frac{F_{htrans} + \langle c \rangle (V - dV)}{V} - \langle c \rangle = \frac{F_{htrans} - \langle c \rangle dV}{V} \quad \text{(S5)}$$

where F_{htrans} is the O_3 flux of horizontal transport; V is the original volume of the PRD grids below the ABL; $dV$is the volume of transported parcels. Assume that the length of the region in the x-directions is *dx*, thus,

$$V = S\,dx \tag{S6}$$

where S is the area of the interface. As calculated in the O_3 mass budget, in the unit time,

$$F_{htrans} = cuS \tag{S7}$$

$$dV = uS \tag{S8}$$

where c is O_3 concentration in the transported air parcels, and u is the mean horizontal wind speed in the interface. Therefore, from Eqs. (S5)-(S8), we can get:

$$\left[\frac{\partial\langle c\rangle}{\partial t}\right]_{htrans} = u\frac{\mathrm{c} - \langle c\rangle}{dx} = u\frac{dc}{dx} \tag{S9}$$

For ABL-FT-H, its contributions when V is much higher than dV (this assumption can be normally met when the period is short) are:

$$\left[\frac{\partial\langle c\rangle}{\partial t}\right]_{ABL-FT-H} = \frac{F_{ABL-FT-H} + \langle c\rangle V}{V + dV} - \langle c\rangle \approx \frac{F_{ABL-FT-H} - \langle c\rangle dV}{V} \tag{S10}$$

where $F_{ABL-FT-H}$ is the O_3 flux contributed by ABL-FT-H. In the unit time,

$$F_{ABL-FT-H} = c_h\frac{\partial H}{\partial t}L^2 \tag{S11}$$

$$dV = \frac{\partial H}{\partial t}L^2 \tag{S12}$$

$$V = HL^2 \tag{S13}$$

where c_h is the O_3 concentration in the ABL top; L is the width of the grid cell (equal to the horizontal resolution of the model); H is the ABL height. Therefore, from Eqs. (S10)-(S13),

$$\left[\frac{\partial\langle c\rangle}{\partial t}\right]_{ABL-FT-H} = \frac{c_h - \langle c\rangle}{H}\frac{\partial H}{\partial t} \tag{S14}$$

For ABL-FT-M,

$$\begin{aligned}\left[\frac{\partial\langle c\rangle}{\partial t}\right]_{ABL-FT-M} &= \frac{F_{ABL-FT-M} + \langle c\rangle(V - dV)}{V} - \langle c\rangle \\ &= \frac{F_{ABL-FT-M} - \langle c\rangle dV}{V}\end{aligned} \tag{S15}$$

$F_{ABL-FT-M}$ is the O_3 flux attributed to ABL-FT-M. In the unit time,

$$F_{ABL-FT-M} = c_h\left(u_h\frac{\partial H}{\partial x} + v_h\frac{\partial H}{\partial y} - w_h\right)L^2 \tag{S16}$$

$$dV = \left(u_h\frac{\partial H}{\partial x} + v_h\frac{\partial H}{\partial y} - w_h\right)L^2 \tag{S17}$$

$$V = HL^2 \tag{S18}$$

where u_h, v_h and w_h are the ABL-top wind speeds in the x, y and z-direction, respectively. Therefore, from Eq. (S15-18),

$$\left[\frac{\partial\langle c\rangle}{\partial t}\right]_{ABL-FT-M} = \frac{c_h - \langle c\rangle}{H}\left(u_h\frac{\partial H}{\partial x} + v_h\frac{\partial H}{\partial y} - w_h\right) \quad \text{(S19)}$$

$$\begin{aligned}\left[\frac{\partial\langle c\rangle}{\partial t}\right]_{ABL-FT} &= \left[\frac{\partial\langle c\rangle}{\partial t}\right]_{ABL-FT-H} + \left[\frac{\partial\langle c\rangle}{\partial t}\right]_{ABL-FT-M} \\ &= \frac{c_h - \langle c\rangle}{H}\left(\frac{\partial H}{\partial t} + u_h\frac{\partial H}{\partial x} + v_h\frac{\partial H}{\partial y} - w_h\right) = \frac{w_e\Delta c}{H}\end{aligned} \quad \text{(S20)}$$

where w_e is the entrainment rate of the ABL; Δc is equal to the difference between O_3 concentrations in the FT and ABL. Therefore, for these transport processes, the above formulas (Eqs. (S9), (S14), (S19), and (S20)) are the same as those used in 1-D models (Janssen and Pozzer, 2015; Vilà-Guerau de Arellano et al., 2015), suggesting their applicability in the quantification of the O_3 concentration budget using CTMs modeling results.

Text S3. Model validation of ABL height, wind and O_3 mixing ratio profiles based on the IAGOS dataset

IAGOS (In-service Aircraft of a Global Observing System; https://www.iagos.org) is a global aircraft-based observing system, where state-of-the-art instruments deployed in aircrafts are used to measure reactive gases, greenhouse gases, aerosol and clouds in the troposphere and lower stratosphere (Petzold et al., 2016). Meteorological parameters, including air temperature, wind speed and direction, are also provided by IAGOS. When the aircrafts climb up or descent, these measurements are suitable for obtaining the vertical profiles of parameters with high resolutions, which provides valuable observational datasets for the model validation in the vertical direction.

To ensure reasonable quantifications of the O_3 budgets, the IAGOS dataset in two representative months in Hong Kong (located in the south PRD) was used to evaluate the modeling performance of WRF-CMAQ in this study. We focused on comparing parameters within the height range of 0-5 km. Since observational data is often missing in some height ranges and the vertical resolution of modeling results is relatively low, we calculated the mean observational and modeling values within every 500 m height range (i.e., 0-500 m, 500-1000 m, etc.) for the comparisons. The detailed evaluations are introduced as follows:

(1) Atmospheric boundary layer (ABL) heights:

ABL heights are used to quantify the contribution of ABL-FT exchange in the O_3 budgets. Therefore, the evaluation of modeled ABL heights is important. In this study, the observational ABL heights were determined using the profiles of potential temperature (θ) in IAGOS, defined as the heights where the lapse rate of θ ($\partial\theta/\partial z$, the rate of θ changing over height change) reaches its maximum values (Dai et al., 2014). Since there are limited profiles available in July 2016 and night-time ABL heights are hard to be accurately determined, we only evaluated the modeling performance of ABL heights during the daytime (6:00-18:00 Local Time (LT)) of Oct. 2015. As shown in Fig. S8, the mean bias (MB) between modeling and observational ABL heights in Hong Kong is only -1.1 m, and a good correlation between ABL heights from two datasets (R = 0.76) suggests that the mean diurnal cycles of ABL can be modeled well. Though the modeling performance of ABL heights is satisfying based on the IAGOS dataset in Hong Kong, more comprehensive comparisons based on three-dimensional observations with higher spatiotemporal resolutions and coverages are required for more accurate O_3 budget estimates in future studies.

(2) Wind profiles:

Figure S9 shows the IAGOS and modeling wind roses within the height ranges of 0-1000 m, 1000-2000 m and 2000-5000 m. Both datasets indicate that higher wind speed can be generally found at higher altitudes. In autumn, WRF overestimates wind speed below 1000 m by 0.6 m/s (16%), but underestimates it above 1000 m. In summer, the biases between wind speeds in the two datasets are relatively smaller, especially at lower heights (< 2000 m). Both datasets show similar prevailing wind directions at different height ranges and in different seasons. Thus, the modeling performance of wind speeds and directions in the vertical direction is acceptable.

(3) O_3 mixing ratio profiles:

The comparisons between observational and modeling profiles of O_3 mixing ratio are displayed in Fig. S10. Not many O_3 profiles were available in July 2016, and the useable ones were mostly measured during clean periods. Thus, the comparison was mainly based on the results in Oct. 2015 (the number of IAGOS O_3 profiles available for the comparisons is 41). Both datasets show that O_3 mixing ratio decreases with height in Hong Kong. Below the height of 1000 m, the observational and modeling O_3 mixing ratios are 71.4 ppbv and 75.8 ppbv, respectively. Within the height range of 1000-2000 m, the O_3 mixing ratio is overestimated by 26%. High O_3 levels during Oct. 13-24 and relatively low O_3 levels in other periods can be found in both datasets, suggesting that the developments of O_3 pollution in the month were modeled well. Therefore, the performance of O_3 profiles modeling can also meet the requirement of O_3 budget calculations.

Text S4. Further analyses on the contributions of horizontal transport and ABL-FT-M in O_3 mass and concentration budgets

(Note: ABL-FT-M, the exchange between ABL and FT due to large-scale air motions (advection through the ABL top).)

As shown in Fig. 3 in the manuscript of this paper, the contributions of both horizontal transport and ABL-FT-M in both O_3 budgets were less notable than those of ABL-FT-H and gas-phase chemistry. However, they reflect the characteristics of regional wind fields, thus are still worthy of further analyses. Two main findings are described as follows:

(1) <u>The contribution of horizontal transport and ABL-FT-M in autumn is connected to the characteristics of horizontal wind fields in the PRD.</u>

Northerly and easterly winds prevail in autumn (Fig. S9), thus O_3 is transported into the PRD through its north and east borders, out of the PRD through the south and west borders, which has been shown in the results of the O_3 mass budget. O_3 outfluxes were generally higher than influxes in the daytime, which is attributed to higher O_3 levels in the air parcels transported out of the PRD than these in parcels into the region. This is also why horizontal transport leads to the decrease of O_3 concentration in the daytime. Though horizontal transport contributed to lower O_3 fluxes at night, it became the main nighttime source for O_3. This is to say, the transport of air parcels with high O_3 levels from the outskirts helped maintain O_3 pollution in the PRD to some extent at night.

The contributions of ABL-FT-M are related to the prevailing of northerly winds in the PRD. The PRD has mountainous regions in the northern, western and eastern outskirts, as well as urban regions with lower altitudes in the central plain. Thus, north winds resulted in the downward transport of O_3 along the terrain. Daytime ABL heights in urban regions were, in general, higher than those in mountainous regions, which is the other reason why O_3 can be easily transported

through the ABL top in the urban-rural interfaces when north wind prevailed. ABL-FT-M contributed to the increase of O_3 concentration during several hours after sunrise and the decrease of O_3 concentration in the afternoon, which is attributed to different comparison results between ABL and FT O_3 levels in two periods (ABL < FT in the morning; ABL > FT in the afternoon).

(2) The contribution of horizontal transport and ABL-FT-M in summer indicates the influence of sea breezes in the PRD.

Although southerly winds normally prevail in summer in the PRD (Fig. S9), on O_3 polluted days, air parcels from other directions could potentially influence the region as well (Qu et al., 2021), resulting in relatively lower horizontal transport fluxes of O_3 in comparison to these in autumn. What interests us is the different contributions of horizontal transport through the southern border of the PRD before and after ~14:00 LT. Besides, we also found high O_3 fluxes contributed by ABL-FT-M in the afternoon. These phenomena are both related to the influence of sea breezes in the PRD.

Figure S11 shows the near-ground wind roses at 14:00, 16:00 and 18:00 LT of O_3 polluted days in July 2016 based on the observational and modeling results in national meteorological sites within the PRD. At 14:00 LT, the main wind directions were W, SW and NW in both datasets. More S and SE winds occurred in later hours, and they became the prevailing winds at 18:00 LT — it suggests the gradual development of sea breezes in the PRD. Thus, O_3 was originally transported out of the PRD through its south border (O_3 fluxes < 0), but sea breezes gradually reversed the directions of O_3 transport, finally resulting in positive O_3 fluxes through the south border in the late afternoon. Sea breezes resulted in the changes of not only horizontal wind fields, but also vertical wind fields. Take the O_3 polluted day July 24th for example, and the cross-section of O_3 concentrations and wind fields in the PRD at 16:00 LT is shown in Fig. S12 (cross-sections were made along the 113.2° E latitude line, from 26.0 to 20.0° N). Sea breezes can be found in this plot, characterized by strong southerly wind and lower O_3 concentrations in the south part of the PRD. In regions where sea breezes and local air parcels encountered (characterized by the interface between low and high O_3 levels), updrafts occurred, suggesting the formation of sea breeze front (Ding et al., 2004; You and Fung, 2019). It promoted the upward transport of O_3 from the ABL to the FT, or considerable O_3 outfluxes attributed to ABL-FT-M.

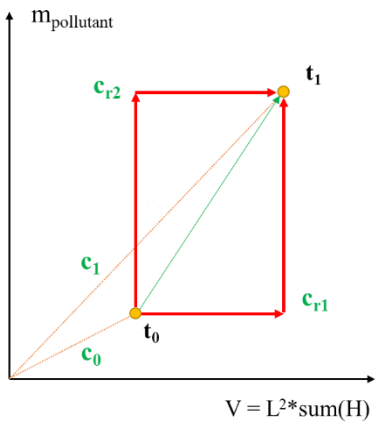

321

322 **Figure S1.** Two calculation paths in the calculation of regional O_3 concentration budget within an
323 hour. $m_{pollutant}$ indicates the total mass of pollutants in the atmospheric boundary layer (ABL) of
324 the studied region; V is the volume of the ABL of the region; L is the length of the grids (equal to
325 the horizontal resolution of the model); H is the ABL heights; t_0 and t_1 are the starting and end
326 hours; c_0 and c_1 are the concentrations of pollutants in t_0 and t_1, respectively; c_{r1} and c_{r2} are the
327 reference concentrations of pollutants for two calculation paths.

328

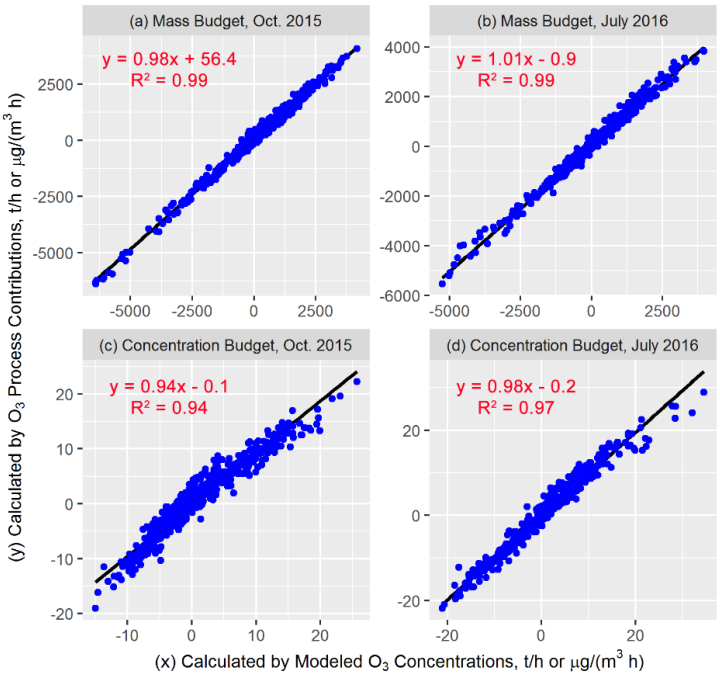

329

330 **Figure S2.** O_3 budget closure examinations in Oct. 2015 (a,c) and July 2016 (b,d), for the O_3
331 mass budget (a-b) and concentration budget (c-d). The units for the O_3 mass and concentration
332 budgets are t/h and μg/(m^3 h), respectively.

333

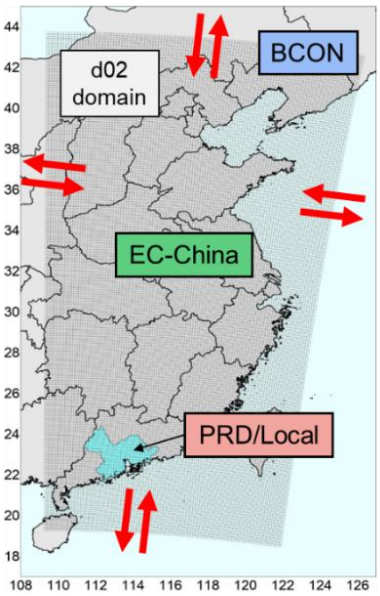

Figure S3. The spatial distributions of the d02 modeling domain and source regions. PRD, Pearl River Delta; EC-China, East and Central China; BCON, the boundary conditions of d02 modeling, or the contributions of sources outside d02.

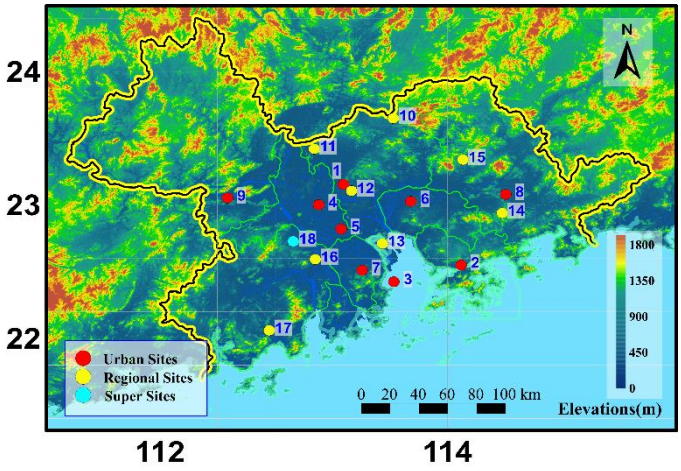

Figure S4. Spatial distributions of 18 sites of the Guangdong-Hong Kong-Macao Pearl River Delta Regional Air Quality Monitoring Network. The names of all sites and their located municipalities are: 1. Luhu, Guangzhou; 2. Liyuan, Shenzhen; 3. Tangjia, Zhuhai; 4. Huijingcheng, Foshan; 5. Jinjuju, Foshan; 6. Nanchengyuanling, Dongguan; 7. Zimaling, Zhongshan; 8. Xiapu, Huizhou; 9. Chengzhongzizhan, Zhaoqing; 10. Tianhu, Guangzhou; 11. Zhudong, Guangzhou; 12. Modiesha, Guangzhou; 13. Wanqingsha, Guangzhou; 14. Jinguowan, Huizhou; 15. Xijiao, Huizhou; 16. Donghu, Jiangmen; 17. Duanfen, Jiangmen; 18. Heshan Supersite, Jiangmen.

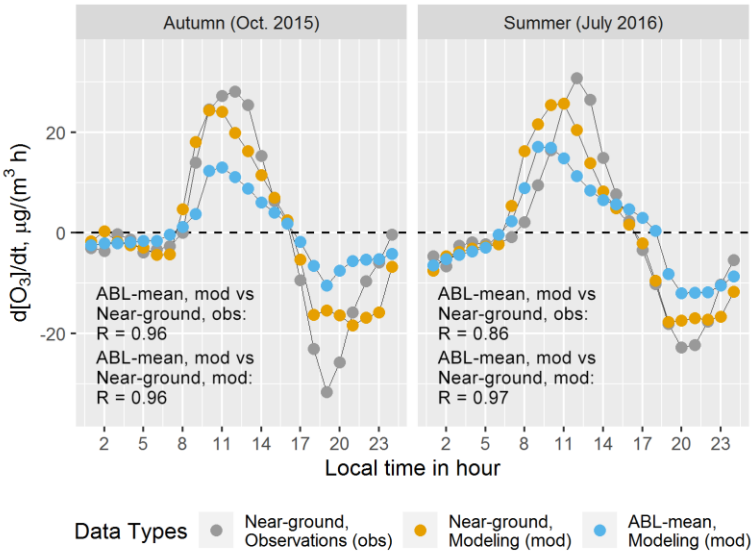

Figure S5. Mean diurnal change of the hourly variations of observational, modeling mean near-ground O_3 concentrations in 18 sites of the Guangdong-Hong Kong-Macao regional monitoring network and modeling mean O_3 concentration over the atmospheric boundary layer (ABL) of the Pearl River Delta on the polluted days of autumn (Oct. 2015) and summer (July 2016).

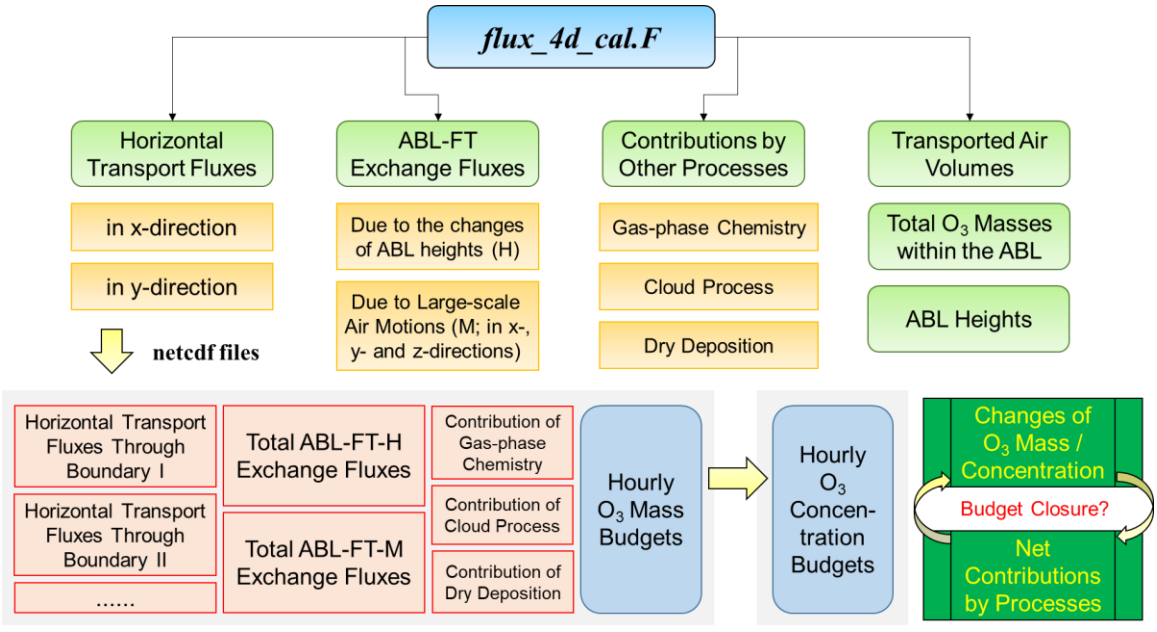

Figure S6. Flow diagram of the O_3 budget calculation processes. ABL, atmospheric boundary layer; FT, free troposphere; ABL-FT-H, ABL-FT exchange due to the changes of ABL height; ABL-FT-M, ABL-FT exchange due to the large-scale air motions (advection through the ABL top).

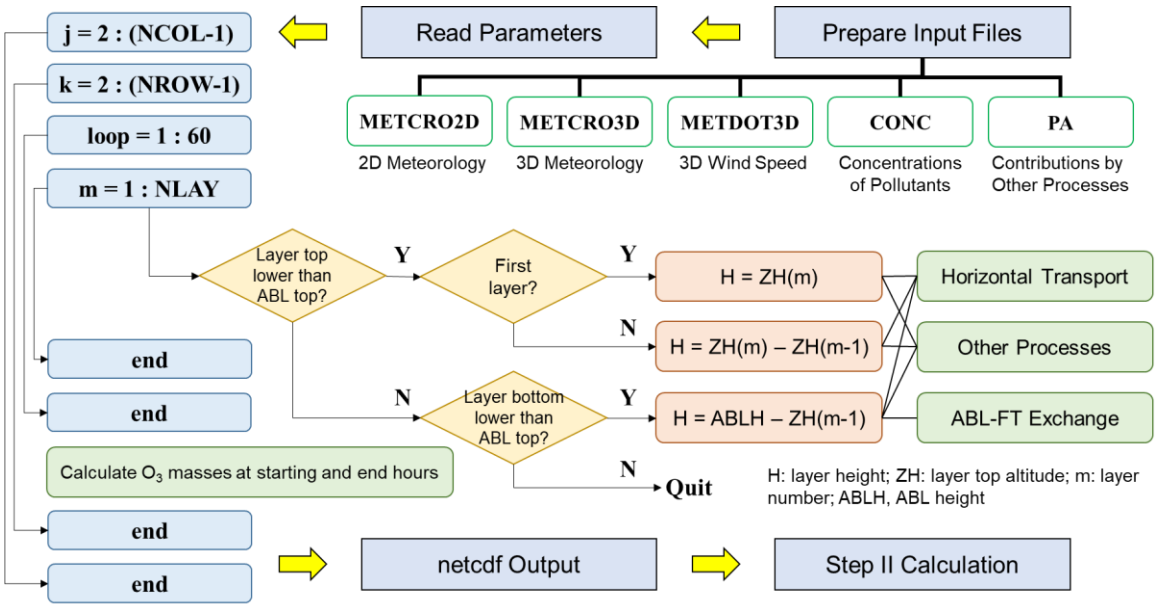

Figure S7. Flow diagram of the O_3 budget calculation in the Step I (or the tool *flux_4d_cal*). NCOL, NROW and NLAY indicate the number of columns, rows and vertical layers in the modeling domain. ABL, atmospheric boundary layer; FT, free troposphere. METCRO2D, 2-dimensional meteorological outputs from the MCIP module in CMAQ; METCRO3D, 3-dimensional meteorological outputs from the MCIP module in CMAQ; METDOT3D, 3-dimensional wind fields outputs from the MCIP module in CMAQ; CONC, 3-dimensional outputs of pollutant concentrations from CMAQ; PA, 3-dimensional outputs of hourly contributions by three non-transport processes to O_3 from CMAQ.

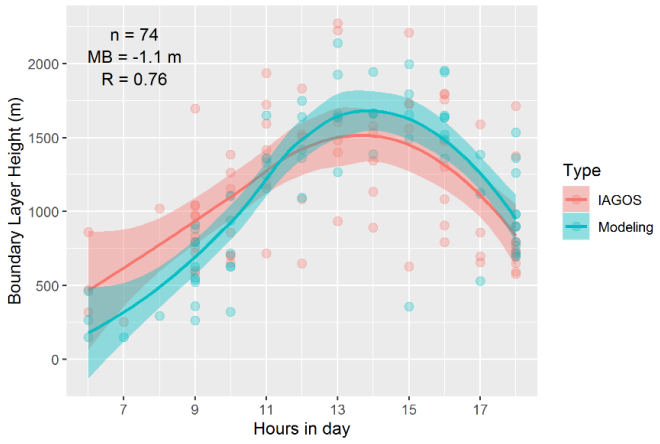

Figure S8. Comparisons between IAGOS and modeling atmospheric boundary layer height in Hong Kong in Oct. 2015. n, the number of available dataset for the comparison; MB, mean bias; R, correlation factor.

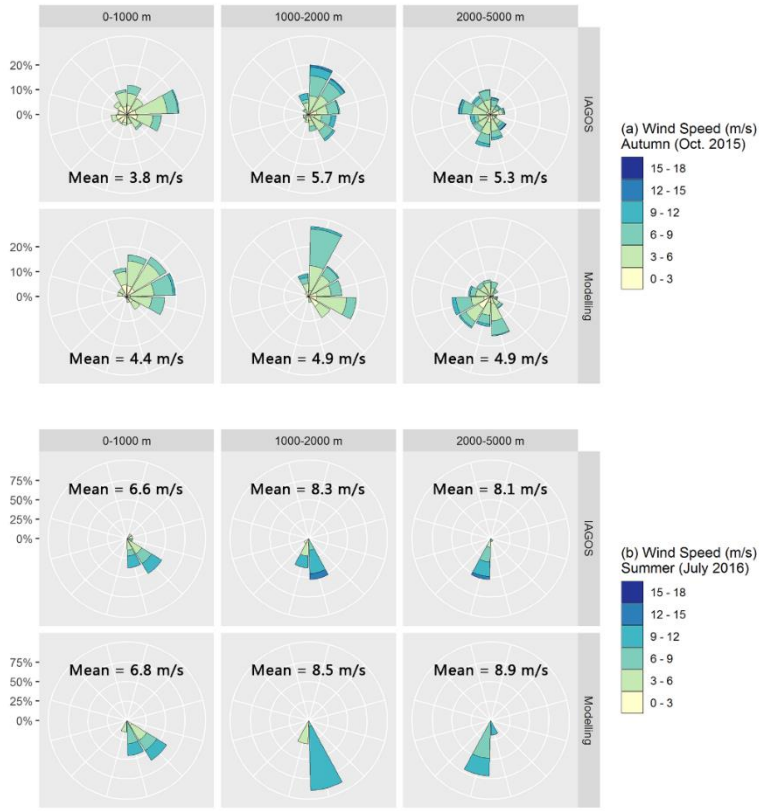

Figure S9. Comparisons between IAGOS and modeling wind roses in Hong Kong in (a) Oct. 2015 and (b) July 2016. Results within the height range of 0-1000 m, 1000-2000 m, and 2000-5000 m were separately displayed.

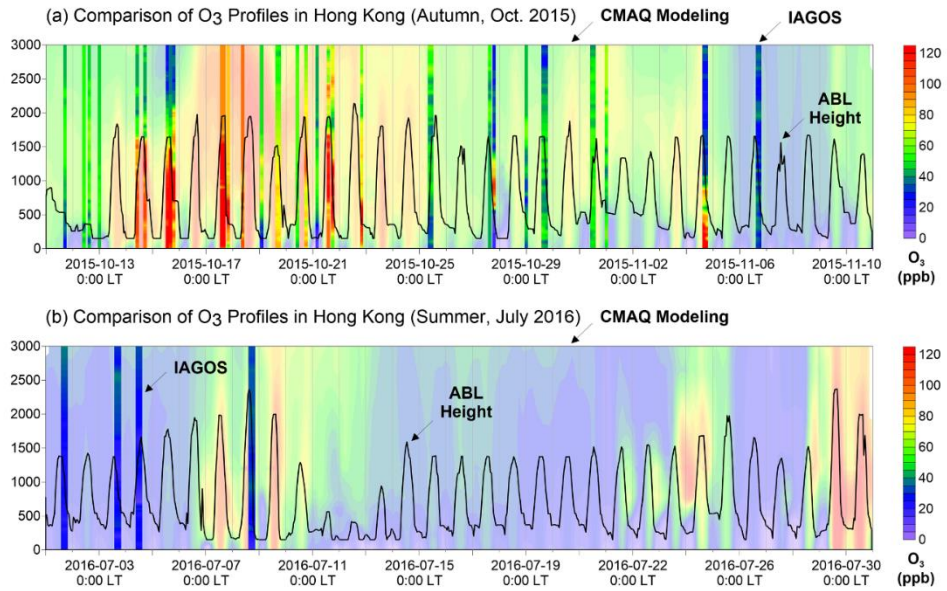

Figure S10. Comparisons between IAGOS and CMAQ modeling vertical profiles of O_3 mixing ratios (ppb) in Hong Kong in (a) Oct. 2015 and (b) July 2016. The heights of atmospheric boundary layer (ABL) modeled by WRF in two months are also shown as solid black lines.

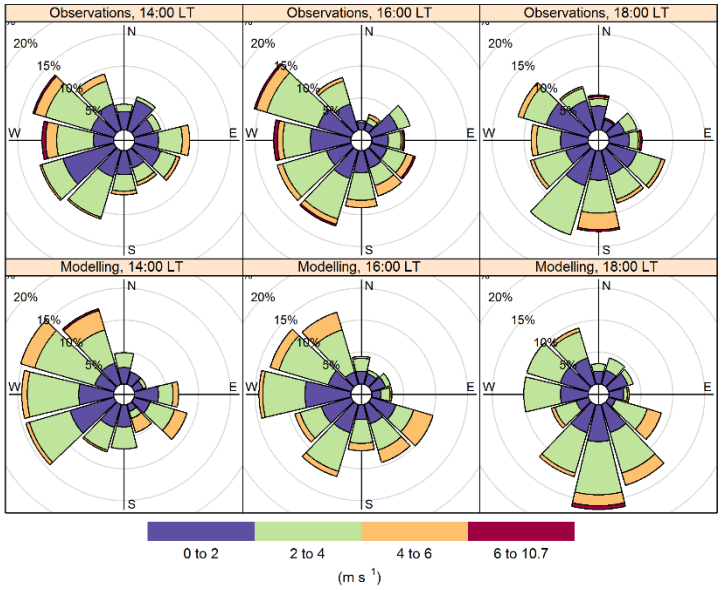

Figure S11. Wind roses at 14:00, 16:00, and 18:00 local time (LT) of O_3 polluted days in July 2016 in the Pearl River Delta (PRD). Observational and modeling wind speeds and directions in 29 national meteorological sites within the PRD were used for this figure.

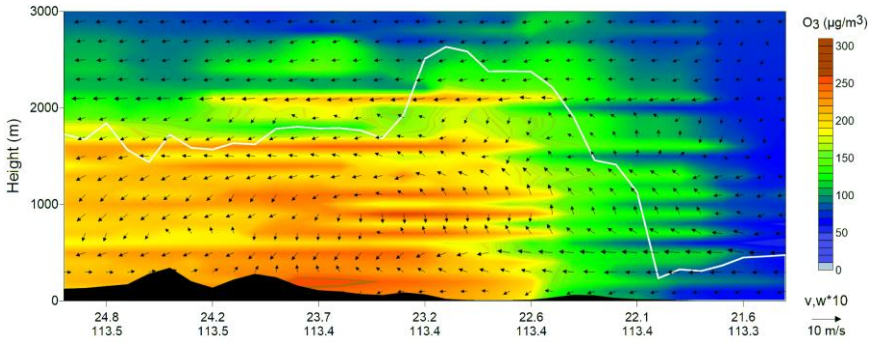

Figure S12. Cross-section of O_3 concentrations (μg/m^3) and wind fields at 16:00 local time on July 24th, 2016. The solid white line indicates the top of the atmospheric boundary layer.

Table S1. Information on the O_3 polluted days of the Pearl River Delta (PRD) in Oct. 2015 and July 2016. MDA1, the maximum 1-hr O_3 concentrations; MDA8, the maximum 8-hr average O_3 concentrations.

Dates	Influencing Weather Systems	O_3 concentrations in the PRD (the maximum values in nine municipals of the PRD, released by the China National Environmental Monitoring Centre; μg/m^3)	
		MDA1	MDA8
Oct.13, 2015	Typhoon Koppu and Champi	201	164
Oct.14, 2015		301	244
Oct.15, 2015		271	227
Oct.16, 2015		260	219
Oct.17, 2015		233	211
Oct.18, 2015		205	187
Oct.19, 2015		214	174
Oct.20, 2015		200	158
Oct.21, 2015		214	195
Oct.22, 2015		209	182
Oct.23, 2015		249	199
Oct.24, 2015		225	193
Oct.28, 2015	Subtropical High	238	186
Nov.3, 2015	Sea High	207	162
Nov.4, 2015		182	168
Nov.5, 2015		255	187
July 7, 2016	Typhoon Nepartak	297	256
July 8, 2016		260	198
July 9, 2016		263	231
July 10, 2016		211	150
July 22, 2016	Subtropical High	211	176
July 23, 2016		223	197
July 24, 2016		265	226
July 25, 2016		334	269
July 26, 2016		235	164
July 29, 2016		271	204
July 30, 2016	Typhoon Nida	268	187
July 31, 2016		385	344

Table S2. Formulas in the O_3 flux calculations for the grid cell (i, j) in the unit time dt, parameters used and their source files in the *flux_4d_cal* tool.

Processes	Formulas of O_3 fluxes	Parameters used	Sources of parameters
Horizontal transport (in the x-direction)	$F_{u-trans} = \sum_{k=1}^{h} c_{i-1,j} u_{i,j+\frac{1}{2}} L \Delta z dt$	$c_{i-1,j}$: O_3 concentrations in the grid cell (i-1, j)	CONC files
		$u_{i,j+\frac{1}{2}}$: wind speeds in the west interface	METDOT3D files
		L: the length of grid cells (= model resolution)	User defined
		Δz: layer heights ($H - z_{h-1}$ for the ABL top layer, $z_k - z_{k-1}$ for other layers within the ABL; H, ABL height)	METCRO3D files
		h: the layer of ABL top	Determined by ABL height
Horizontal transport (in the y-direction)	$F_{v-trans} = \sum_{k=1}^{h} c_{i,j-1} v_{i+\frac{1}{2},j} L \Delta z dt$	$c_{i,j-1}$: O_3 concentrations in the grid cell (i, j-1)	CONC files
		$v_{i+\frac{1}{2}j}$: wind speeds in the south interface	METDOT3D files
		L: the length of grid cells (= model resolution)	User defined
		Δz: layer heights ($H - z_{h-1}$ for the ABL top layer, $z_k - z_{k-1}$ for other layers within the ABL; H, ABL height)	METCRO3D files
		h: the layer of ABL top	Determined by ABL height
ABL-FT exchange due to the changes of ABL heights	$F_{ABL-FT-H} = c_h \frac{\partial H}{\partial t} L^2 dt$	c_h: O_3 concentrations in the ABL top layer	CONC files
		$\frac{\partial H}{\partial t}$: the change rates of ABL height	METCRO2D files
		L: the length of grid cells (= model resolution)	User defined
ABL-FT exchange due to large-scale air motions (in the x-direction)	$F_{ABL-FT-Cu} = c_{i-1,j(h)} u_{i,j+\frac{1}{2}(h)} \frac{\partial H}{\partial x} L^2 dt$	$c_{i-1,j(h)}$: O_3 concentrations in the ABL top layer of the grid cell (i-1, j)	CONC files
		$u_{i,j+\frac{1}{2}(h)}$: wind speeds in the ABL top layer of the west interface	METDOT3D files
		L: the length of grid cells (= model resolution)	User defined
		$\frac{\partial H}{\partial x}$: the difference of ABL heights in x-direction, or between the grid cells (i, j) and (i-1, j)	METCRO2D files
ABL-FT exchange due to large-scale air motions (in the y-direction)	$F_{ABL-FT-Cv} = c_{i,j-1(h)} v_{i+\frac{1}{2},j(h)} \frac{\partial H}{\partial y} L^2 dt$	$c_{i,j-1(h)}$: O_3 concentrations in the ABL top layer of the grid cell (i, j-1)	CONC files
		$v_{i+\frac{1}{2},j(h)}$: wind speeds in the ABL top layer of the south interface	METDOT3D files
		L: the length of grid cells (= model resolution)	User defined
		$\frac{\partial H}{\partial y}$: the difference of ABL heights in y-direction, or between the grid cells (i, j) and (i, j-1)	METCRO2D files
ABL-FT exchange due to large-scale air motions (in the z-direction)	$F_{ABL-FT-Cw} = -c_h w_h L^2 dt$	c_h: O_3 concentrations in the ABL top layer	CONC files
		w_h: vertical wind speeds in the ABL top layer	METCRO3D files
		L: the length of grid cells (= model resolution)	User defined
Other processes (gas-phase chemistry, cloud process, dry deposition)	$F_{others} = \sum_{k=1}^{h} IPR \Delta z dt$	IPR: integrated process rates of pre-set processes	PA files
		Δz: layer heights ($H - z_{h-1}$ for the ABL top layer, $z_k - z_{k-1}$ for other layers within the ABL; H, ABL height)	METCRO3D files
		h: the layer of ABL top	Determined by ABL height